*Complex Planetary Systems II: Latest Methods for an Interdisciplinary Approach*
*Proceedings IAU Symposium No. 382, 2024*
*A. Lemaitre & A.-S. Libert, eds.*
doi:10.1017/S1743921323004192

# Excitation of the obliquity of Earth-like planets via tidal forcing using the Andrade rheology

**Ema F. S. Valente**[1] **and Alexandre C. M. Correia**[1,2]

[1]CFisUC, Departamento de Física, Universidade de Coimbra, 3004-516 Coimbra, Portugal
email: emavalente@ua.pt

[2]IMCCE, Observatoire de Paris, PSL Université, 77 Av. Denfert-Rochereau, 75014 Paris, France

**Abstract.** Close-in planets undergo strong tidal effects with their host stars that modify their spins and orbits. Adopting a Maxwell rheology, it has been shown that for the 5/2 and 7/2 spin-orbit resonances, the obliquity of these planets can stabilise at a high value. Here, we show that these high obliquity metastable states can also be observed for the same spin-orbit resonances considering the Andrade rheology.

**Keywords.** planet-star interactions, dynamical evolution and stability, terrestrial planets

## 1. Introduction

Many exoplanets have been discovered in the habitable zone of low-mass stars, especially around M-dwarf stars. These stars comprise $\sim 70\%$ of all stars in the Milky Way (Bochanski et al. 2010), and the occurrence rate of Earth-sized planets is higher than around other main sequence stars (Tuomi et al. 2019). Furthermore, the detection of small planets is easier via radial velocity and transit techniques.

The search for habitable worlds around M-dwarf stars has some advantages. The habitable zone is closer to the star due to its low luminosity and these stars are the longest-living stars in the Universe, which could provide enough time for biological development. Yet, it has one major disadvantage. In the M-dwarfs planetary systems, the tidal interactions between the planet and the star are strong, which can lead the planet to develop synchronous rotation (the rotation period matches the orbital period) and zero obliquity (Hut 1980). This configuration is not ideal for the habitability.

Valente and Correia (2022) have studied the tidal evolution of these planetary systems and found that, in a two-body problem, the synchronous rotation can be prevented, and stabilisation on spin-orbit resonances with high obliquity states can occur. However, to handle the deformation of the planet, they only assume a Maxwell rheology. Here, we extend the work presented in Valente and Correia (2022) by adopting an Andrade rheological model (for a review of these and other main viscoelastic models, see Renaud and Henning 2018).

## 2. Model

We consider a system composed of a planet with mass $m$ and a star with mass $M_\star$. The planet is an extended body with radius $R$ and rotates with angular velocity $\omega = \omega\,\mathbf{s}$.

It can be deformed under the action of tides, which gives rise to the tidal potential (e.g. Lambeck 1980),

$$V(\mathbf{r}) = -k_2 \frac{\mathcal{G} M_\star}{R} \left(\frac{R}{r}\right)^3 \left(\frac{R}{r_\star}\right)^3 P_2\left(\frac{\mathbf{r}\cdot\mathbf{r}_\star}{r\, r_\star}\right) , \tag{1}$$

where $\mathcal{G}$ is the gravitational constant, $\mathbf{r}$ is the distance measured from the planet's centre of mass, $\mathbf{r}_\star$ is the position of the star, $P_2(x) = (3x^2 - 1)/2$ is a Legendre polynomial, and $k_2$ is the second Love number for potential, that depends on the internal structure of the planet and is a function on the frequency of the perturbation, $\sigma$.

We obtain the spin and orbital equations of motion from the torque, $\mathbf{T} = -M_\star \mathbf{r}_\star \times \nabla V(\mathbf{r}_\star)$, and from the power, $\dot{E} = -M_\star \dot{\mathbf{r}}_\star \cdot \nabla V(\mathbf{r}_\star)$. Tidal effects slowly modify the spin and the orbit of the planet in a timescale much longer than the orbital and precession periods of the system. Thus, we can average the torque and the power over the mean anomaly and the argument of pericentre as

$$\left\langle \mathbf{T} \right\rangle = T_p\, \mathbf{p} + T_q\, \mathbf{q} + T_s\, \mathbf{s} \quad \text{and} \quad \left\langle \dot{E} \right\rangle = n\, T_E, \tag{2}$$

where $n$ is the mean motion, and $T_p, T_q, T_s, T_E$ are expressed in Hansen coefficients, which depend solely on the eccentricity (their full expressions are given in Valente and Correia 2022). $(\mathbf{p}, \mathbf{q}, \mathbf{s})$ is a set of orthogonal vectors, where $\mathbf{p} = \mathbf{k} \times \mathbf{s}$, $\mathbf{q} = \mathbf{s} \times \mathbf{p}$, and $\mathbf{k}$ is the unit vector normal to the orbital plane (see Correia and Valente 2022).

To handle the deformations of the planet, we need to adopt some rheological model for the second Love number $k_2$. Unlike Valente and Correia (2022), we choose the Andrade model. An Andrade solid is represented by three mechanical elements combined in series: a spring, a dashpot, and a spring-pot (e.g. Andrade 1910). The second Love number for the Andrade model is given by (e.g. Efroimsky 2012):

$$k_2(\sigma) = \frac{k_f}{1 + \tilde{\mu}(\sigma)} , \tag{3}$$

where

$$\tilde{\mu}(\sigma) = \left(\frac{\tau}{\tau_e} - 1\right) \left[1 - i(\sigma\tau_e)^{-1} + (i\sigma\tau_A)^{-\alpha}\, \Gamma(1+\alpha)\right]^{-1} \tag{4}$$

is the effective rigidity. Here $\tau_A$ is the anelastic relaxation time, $\tau_e$ is the Maxwell relaxation time, and $\tau = k_f \tau_e / k_e$ is a global relaxation time, where $k_f$ and $k_e$ are the fluid and the elastic Love numbers, respectively. The anelastic relaxation time can also be related to the Maxwell relaxation time, for simplicity we assume that $\tau_A = \tau$ (Efroimsky 2012). The relaxation times are not well determined for the Earth due to uncertainties in the effective viscosity, and so we treat $\tau$ as a free parameter. The $\alpha$ parameter is the time exponent of the Andrade transient creep strain law and is an empirical adjustable parameter whose value depends on the material. We usually have $0.2 \leq \alpha \leq 0.4$ for rocky planets (Castillo-Rogez et al. 2011), but $\alpha = 1$ for the Maxwell model. The dissipation of the system is only given by the imaginary part of Eq. (3).

In the following, we explore the secular tidal evolution of the planet (Eq. (2)) for different values of $\alpha$, eccentricities, and $\tau$ values, in order to observe possible configurations where the Earth-like planets can have non-synchronous rotation rates and high obliquity states, as was observed with the Maxwell rheology (see Valente and Correia 2022).

## 3. Spin dynamics

Independently of the tidal model that we adopt, the final state of tidal evolution corresponds to circular orbits, zero obliquity, and synchronous rotation (Hut 1980). However, the spin evolves much faster than the orbit (Valente and Correia 2022), and so in this

https://doi.org/10.1017/S1743921323004192 Published online by Cambridge University Press

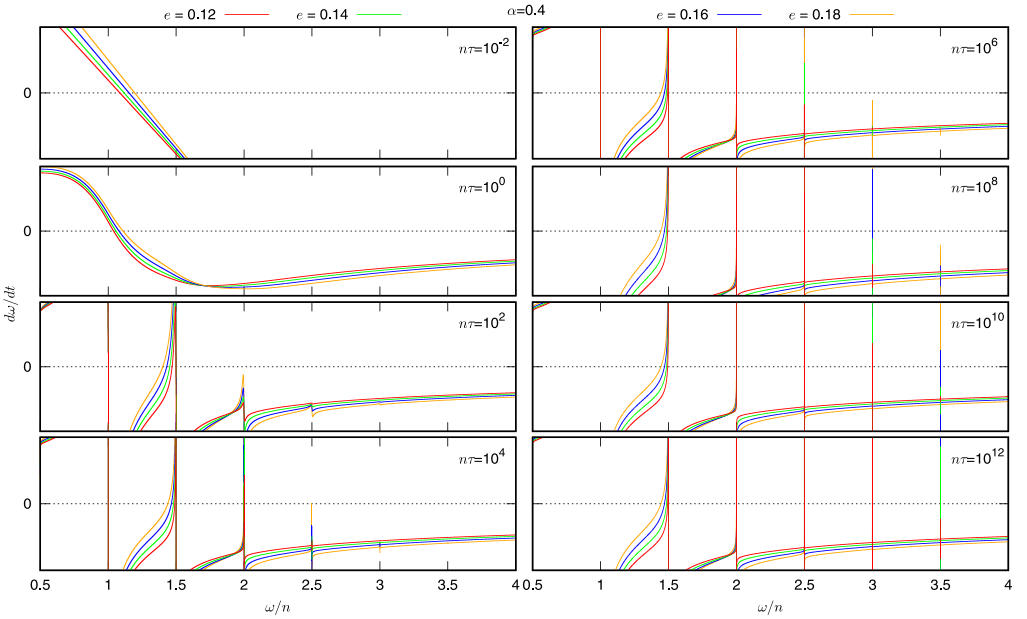


**Figure 1.** Variation of $d\omega/dt$ with $\omega/n$, assuming the Andrade rheology with $\alpha = 0.4$, for different values of $n\tau$ and four different eccentricities: $e = 0.12$ (red), $e = 0.14$ (green), $e = 0.16$ (blue), and $e = 0.18$ (orange). We adopt here $\theta = 0$.

section, we assume that the eccentricity and semi-major axis are constant. We thus only consider the spin evolution given by the rotation rate, $\omega$, and the obliquity, $\theta$,

$$\frac{\dot{\omega}}{\omega} = -\frac{T_s}{C\omega} \quad \text{and} \quad \dot{\theta} \approx \frac{T_q}{C\omega}\sin\theta\,, \tag{5}$$

respectively, where $C = \xi m R$ is the principal moment of inertia of the planet, and $\xi$ is an internal structure constant. Also, we limit our analysis to positive rotation rates ($\omega > 0$). Our main goal is to describe the possible equilibria and evolutionary paths for different tidal regimes (different $\tau$ values).

### 3.1. *Equilibrium rotation*

The final evolution of the spin has zero obliquity, which is an equilibrium point (Eq. (5)). Therefore, we initially assume $\theta = 0$ (planar case). In Fig. 1, we plot, as an example, the evolution of the rotation rate for $\alpha = 0.4$ as a function of $\omega/n$ for different values of eccentricities and $n\tau$. The interception with the horizontal dotted line $\dot{\omega} = 0$ gives all the equilibria for the rotation rate. Negative slopes correspond to stable equilibria, where the rotation can remain locked for a given value of the eccentricity. We adopt eccentricity values between $e = 0.12$ and $e = 0.18$, and vary $n\tau$ with the power $10^N$ up to $N = 12$. These values are not exactly the same as in Valente and Correia (2022) for the Maxwell model, because in the nonlinear regime, for the same $n\tau$ value, the Andrade model dissipates more energy.

For $n\tau \lesssim 1$, we observe that a single stable equilibrium point exists, close to synchronous rotation, which is known as the pseudo-equilibrium rotation. For $n\tau \gg 1$, additional stable equilibria appear. They cluster around semi-integer values, known as spin-orbit resonances, because $\dot{\omega}$ has extrema at these values. When the amplitude of $\dot{\omega}$ surpasses the line $\dot{\omega} = 0$, the rotation can be locked in that spin-orbit resonance. Here,

https://doi.org/10.1017/S1743921323004192 Published online by Cambridge University Press

we also observe that by increasing $n\tau$ and/or the eccentricity, the number of spin-orbit equilibria increase.

Although we only show here the example for $\alpha = 0.4$, by changing this parameter, we note a difference in the first capture in a given spin-orbit resonance for the same $n\tau$ value. By comparing our Fig. 1 with Fig.1 of Valente and Correia (2022), for instance, for $n\tau = 10^4$ and $e = 0.16$, in our Fig. 1 ($\alpha = 0.4$), the first capture occurs in the 2/1 resonance, while in Fig.1 of Valente and Correia (2022) (which is equivalent to $\alpha = 1$), the first capture occurs in the 3/1 resonance. Therefore, we conclude that the value of $\alpha$ modifies the captures in spin-orbit resonances. This is why we need to show higher values of $n\tau$, because by decreasing the value of $\alpha$, the capture in a given spin-orbit resonance can only occur for higher values of $n\tau$.

In Fig. 1, we also observe that for the same $n\tau$ value, stabilisation can occur at different spin-orbit resonances, depending on the eccentricity. Here, we assume a constant eccentricity, yet it also evolves slowly with time (Valente and Correia 2022). By decreasing the eccentricity value, the higher-order spin-orbit equilibria become unstable, and the rotation is sequentially captured in lower-order resonances.

### 3.2. *Equilibrium obliquity*

Despite $\theta = 0$ being an equilibrium point (Eq. (5)), it is not necessarily stable. For $T_q > 0$, the equilibrium point can be unstable, and the obliquity is allowed to grow. To find these additional stable equilibrium states, we compute numerically the rotation and obliquity rates (Eq. (5)), determining the pair $(\omega/n, \theta)$ that simultaneously satisfy $T_q = T_s = 0$.

In Fig. 2, we compute the high obliquity stable equilibria for $\alpha = 0.2$, 0.3, 0.4, 0.5 and 0.6, and also the high obliquity state equilibria for the Maxwell rheology ($\alpha = 1$). We observe that for $\omega/n \approx 5/2$ and $\omega/n \approx 7/2$ also exist high obliquity states as in the case with the Maxwell model (Valente and Correia 2022). However, for $\alpha = 0.2$, the high obliquity state only exists for $\omega/n \approx 5/2$. These states do not directly depend on the value of $n\tau$, but they become unstable below some critical eccentricity, which depends on $n\tau$. We observe that as we increase the $n\tau$ value, the critical eccentricity becomes smaller. We mark with a dot the critical eccentricity for $n\tau = 10^N$, where the value of $N$ is given next to the dot. By increasing the value of $\alpha$, the high obliquity state curves of the 5/2 and 7/2 resonances widen, englobing more eccentricity values and $n\tau$ values. Also, by increasing $\alpha$, high obliquities states exist for lower values of $n\tau$. Indeed, by increasing $\alpha$, we approach the regime of the Maxwell rheology, and the curve tends to be equal to Fig. 2 f. An important difference is that for lower values of $\alpha$, the maximal obliquity that can be attained is smaller. For instance, for $\alpha = 0.3$, the obliquity can reach nearly 15° for the 5/2 resonance and 11° for the 7/2 resonance, while for $\alpha = 0.6$, the obliquity can reach nearly 62° for the 5/2 resonance and 49° for the 7/2 resonance.

## 4. Aplication to Proxima b

We now apply our model to the long-term tidal evolution of Proxima Centauri b, a planet with mass $m = 1.17\ M_\oplus$, radius $R = 1.08\ R_\oplus$, and semi-major axis $a = 0.049$ au, which is in the habitable zone of a M-dwarf star with mass $M_\star = 0.12\ M_\odot$ (Anglada-Escudé et al. 2016). For the structure and Love numbers, we adopt those of the Earth, $\xi = 0.330$, $k_f = 0.933$ and $k_e = 0.295$ (Yoder 1995). The initial conditions of the spin are a rotation period of 24 h and the obliquity starts at $\theta = 10°$. We only show configurations where the high obliquity equilibria occur when $\alpha$ is in the range of $0.2 \leq \alpha \leq 0.4$ (the usually accepted range for rocky planets).

https://doi.org/10.1017/S1743921323004192 Published online by Cambridge University Press

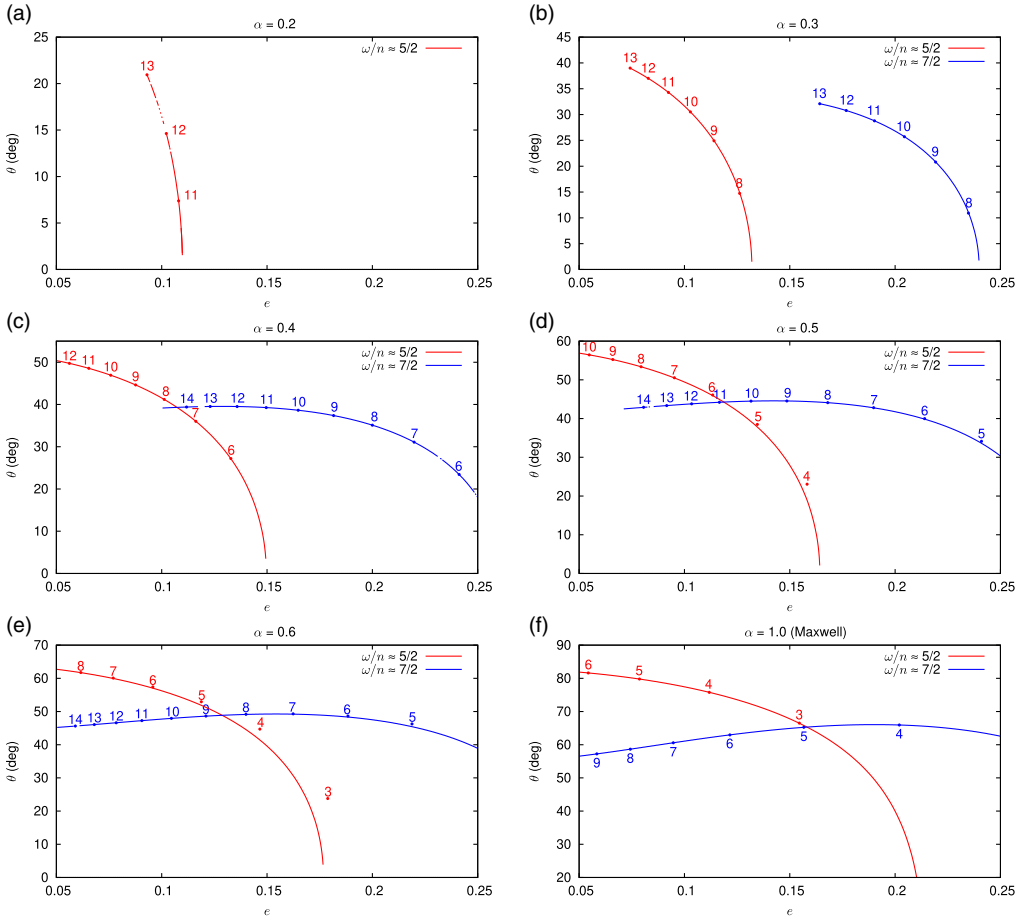


**Figure 2.** High obliquity stable equilibria as a function of the eccentricity for values of $\alpha$ between 0.2 and 0.6, and for the Maxwell model ($\alpha = 1$). The dots mark the critical eccentricity for $n\tau = 10^N$, where the $N$-value is given next to the dot. These states are found numerically by determining the pair $(\omega/n, \theta)$ that simultaneously satisfy $T_q = T_s = 0$.

The results of the simulations are shown in Fig. 3. For each panel, we show the eccentricity (top), the $\omega/n$ ratio (middle), and the obliquity (bottom) as a function of time. We do not present the full tidal evolution of the planet because we are only interested in showing that high obliquity states occur even for the Andrade rheology.

In Fig. 3 a, we show the evolution with $n\tau = 10^6$ for $\alpha = 0.4$ and the initial eccentricity is $e = 0.14$. At the beginning of the evolution, the rotation evolves rapidly towards the 3/1 resonance, where it stays briefly until destabilisation occurs. Then, it is captured in the 5/2 spin-orbit resonance. Here, a high obliquity state is attained for a very short time ($\sim 0.3$ Gyr) with $\theta \approx 25°$. This is only possible for $n\tau > 10^5$ as we have seen in Fig. 2 c. The rotation subsequently evolves into the 2/1 spin-orbit resonance, where the obliquity drops to zero.

In Fig. 3 b we adopt $n\tau = 10^9$ for $\alpha = 0.3$ and the initial eccentricity is $e = 0.12$. Here, the rotation evolves directly into the 5/2 spin-orbit resonance. We observe the slow growth of the obliquity when the planet is captured in this resonance. This high obliquity equilibrium remains stable for $\sim 3$ Gyr until the destabilisation of the 5/2 spin-orbit

https://doi.org/10.1017/S1743921323004192 Published online by Cambridge University Press

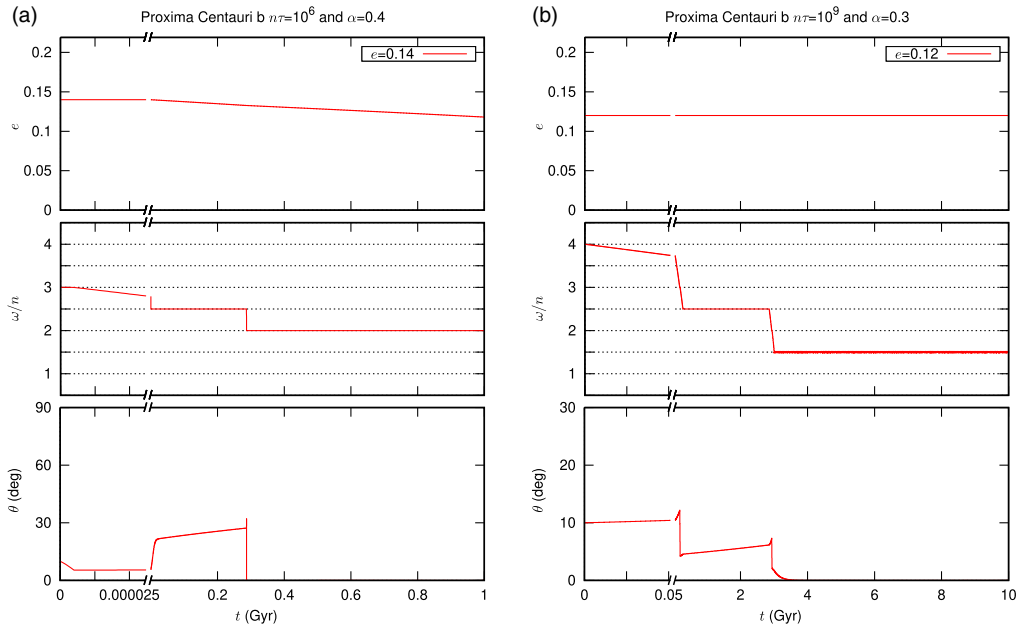


**Figure 3.** Secular evolution over time of Proxima b for a) $\alpha = 0.4$ with $n\tau = 10^6$ and b) $\alpha = 0.3$ with $n\tau = 10^9$; with initial eccentricities a) $e = 0.14$ and b) $e = 0.12$. We show the eccentricity (top), the $\omega/n$ ratio (middle) and the obliquity (bottom). Note the break in the time scale.

resonance occurs. Then, the rotation is captured in the 3/2 resonance and the obliquity descends again to zero. This behavior is also in agreement with Fig. 2 b.

## 5. Conclusion

In this work, we show that when we consider the Andrade rheology instead of the Maxwell one, rocky planets in the habitable zone of low-mass stars can still develop high obliquity states for the specific 5/2 and 7/2 spin-orbit resonances, as described in Valente and Correia (2022). However, these high obliquity states are less likely, because they are only possible for some particular values of the eccentricity and unrealistic large values of $n\tau$. The obliquity also attains lower values and lasts for shorter periods of time, since for the Andrade model the dissipation is higher than in the Maxwell model for the same $n\tau$ value.

**Acknowledgements.** This work was supported by grant SFRH/BD/137958/2018, and by projects CFisUC (UIDB/04564/2020 and UIDP/04564/2020), GRAVITY (PTDC/FIS-AST/7002/2020), and ENGAGE SKA (POCI-01-0145-FEDER-022217), funded by COMPETE 2020 and FCT, Portugal. The numerical simulations were performed at the Laboratory for Advanced Computing at University of Coimbra (https://www.uc.pt/lca).

## References

Andrade, E. N. d. C. 1910, On the Rigidity of the Earth. *Proc. R. Soc. Lond. A*, 84, 1–12.

Anglada-Escudé, G., Amado, P. J., Barnes, J., Berdiñas, Z. M., Butler, R. P., Coleman, G. A. L., de La Cueva, I., Dreizler, S., Endl, M., Giesers, B., Jeffers, S. V., Jenkins, J. S., Jones, H. R. A., Kiraga, M., Kürster, M., López-González, M. J., Marvin, C. J., Morales, N., Morin, J., Nelson, R. P., Ortiz, J. L., Ofir, A., Paardekooper, S.-J., Reiners, A., Rodríguez, E., Rodríguez-López, C., Sarmiento, L. F., Strachan, J. P., Tsapras, Y., Tuomi, M., & Zechmeister, M. 2016, A terrestrial planet candidate in a temperate orbit around Proxima Centauri. *Nature*, 536(7617), 437–440.

https://doi.org/10.1017/S1743921323004192 Published online by Cambridge University Press

Bochanski, J. J., Hawley, S. L., Covey, K. R., West, A. A., Reid, I. N., Golimowski, D. A., & Ivezić, Z. 2010, The luminosity and mass functions of low-mass stars in the galactic disk. ii. the field. *The Astronomical Journal*, 139(6), 2679–2699.

Castillo-Rogez, J. C., Efroimsky, M., & Lainey, V. 2011, The tidal history of Iapetus: Spin dynamics in the light of a refined dissipation model. *Journal of Geophysical Research (Planets)*, 116(E9), E09008.

Correia, A. C. M. & Valente, E. F. S. 2022, Tidal evolution for any rheological model using a vectorial approach expressed in Hansen coefficients. *Celestial Mechanics and Dynamical Astronomy*, 134(3), 24.

Efroimsky, M. 2012, Bodily tides near spin-orbit resonances. *Celestial Mechanics and Dynamical Astronomy*, 112, 283–330.

Hut, P. 1980, Stability of tidal equilibrium. *Astronomy and Astrophysics*, 92, 167–170.

Lambeck, K. 1980,. *The Earth's Variable Rotation: Geophysical Causes and Consequences*. Cambridge University Press.

Renaud, J. P. & Henning, W. G. 2018, Increased Tidal Dissipation Using Advanced Rheological Models: Implications for Io and Tidally Active Exoplanets. *Astrophysical Journal*, 857(2), 98.

Tuomi, M., Jones, H. R. A., Butler, R. P., Arriagada, P., Vogt, S. S., Burt, J., Laughlin, G., Holden, B., Shectman, S. A., Crane, J. D., Thompson, I., Keiser, S., Jenkins, J. S., Berdiñas, Z., Diaz, M., Kiraga, M., & Barnes, J. R. 2019,. Frequency of planets orbiting m dwarfs in the solar neighbourhood.

Valente, E. F. S. & Correia, A. C. M. 2022, Tidal excitation of the obliquity of Earth-like planets in the habitable zone of M-dwarf stars. *Astronomy and Astrophysics*, 665, A130.

Yoder, C. F. Astrometric and geodetic properties of Earth and the Solar System. In *Global Earth Physics: A Handbook of Physical Constants* 1995,, pp. 1–31. American Geophysical Union, Washington D.C.